ACS central science

Research Article

Cite This: ACS Cent. Sci. 2019, 5, 852−866

http://pubs.acs.org/journal/acscii

Broad-Spectrum Proteome Editing with an Engineered Bacterial Ubiquitin Ligase Mimic

Morgan B. Ludwicki,[†,#] Jiahe Li,[‡,§,#] Erin A. Stephens,[∥] Richard W. Roberts,[⊥] Shohei Koide,[▽,○] Paula T. Hammond,[‡,§] and Matthew P. DeLisa*[,†,∥]

[†]Robert F. Smith School of Chemical and Biomolecular Engineering, Cornell University, 120 Olin Hall, Ithaca, New York 14853, United States

[‡]Department of Chemical Engineering and [§]Koch Institute for Integrative Cancer Research, Massachusetts Institute of Technology, Cambridge, Massachusetts 02139, United States

[∥]Biochemistry, Molecular and Cell Biology, Cornell University, Ithaca, New York 14853, United States

[⊥]Department of Chemistry, University of Southern California, Los Angeles, California 90089, United States

[▽]Perlmutter Cancer Center, New York University Langone Medical Center, New York, New York 10016, United States

[○]Department of Biochemistry and Molecular Pharmacology, New York University School of Medicine, New York, New York 10016, United States

Supporting Information

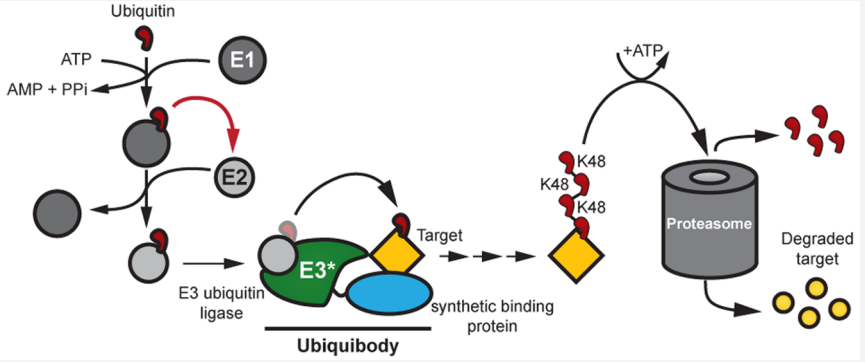

ABSTRACT: Manipulation of the ubiquitin-proteasome pathway to achieve targeted silencing of cellular proteins has emerged as a reliable and customizable strategy for remodeling the mammalian proteome. One such approach involves engineering bifunctional proteins called ubiquibodies that are comprised of a synthetic binding protein fused to an E3 ubiquitin ligase, thus enabling post-translational ubiquitination and degradation of a target protein independent of its function. Here, we have designed a panel of new ubiquibodies based on E3 ubiquitin ligase mimics from bacterial pathogens that are capable of effectively interfacing with the mammalian proteasomal degradation machinery for selective removal of proteins of interest. One of these, the *Shigella flexneri* effector protein IpaH9.8 fused to a fibronectin type III (*FN3*) monobody that specifically recognizes green fluorescent protein (GFP), was observed to potently eliminate GFP and its spectral derivatives as well as 15 different FP-tagged mammalian proteins that varied in size (27−179 kDa) and subcellular localization (cytoplasm, nucleus, membrane-associated, and transmembrane). To demonstrate therapeutically relevant delivery of ubiquibodies, we leveraged a bioinspired molecular assembly method whereby synthetic mRNA encoding the GFP-specific ubiquibody was coassembled with poly A binding proteins and packaged into nanosized complexes using biocompatible, structurally defined polypolypeptides bearing cationic amine side groups. The resulting nanoplexes delivered ubiquibody mRNA in a manner that caused efficient target depletion in cultured mammalian cells stably expressing GFP as well as in transgenic mice expressing GFP ubiquitously. Overall, our results suggest that IpaH9.8-based ubiquibodies are a highly modular proteome editing technology with the potential for pharmacologically modulating disease-causing proteins.

INTRODUCTION

Protein function has traditionally been investigated by disrupting the expression of a target gene encoding a protein and analyzing the resulting phenotypic consequences. Such loss-of-function experiments are now routinely performed using gene silencing and genome editing techniques such as antisense oligonucleotides (ASOs), RNA interference (RNAi), zinc finger nucleases (ZFNs), transcription activator-like effector nucleases (TALENs), and clustered, regularly

Received: February 8, 2019
Published: May 10, 2019

interspaced, short palindromic repeat (CRISPR)-Cas systems.[1−4] These methods are widely used in basic research and hold promise for treating genetic disorders.[4−8] However, a number of challenges remain including lack of temporal control and unpredictable off-target effects; the inability in the case of genome editing to remove essential genes and the irreversible nature of such knockouts; and the inability in the case of gene silencing to decrease levels of proteins already present within cells, thereby leaving stable, long-lived proteins unaffected.

Proteome editing technology represents an orthogonal approach for studying protein function that operates at the post-translational level and has the potential to dissect complicated protein functions at higher resolution than methods targeting DNA or RNA and with post-translational precision. One of the most notable methods involves "inhibition-by-degradation" whereby the machinery of the cellular ubiquitin-proteasome pathway (UPP) is hijacked to specifically degrade proteins of interest. The canonical ubiquitination cascade requires the activities of three enzymes—ubiquitin activating enzyme (E1), ubiquitin-conjugating enzymes (E2), and ubiquitin ligases (E3)—which act sequentially to tag proteins for degradation through the covalent attachment of a poly ubiquitin chain to lysine residues in an energy-dependent manner.

E3s are the most heterogeneous class of enzymes in the UPP (there are >600 E3s in humans) and can be classified as HECT (homologous to E6AP C-terminus), RING (really interesting new gene), and RBR (RING-between-RING) depending on the presence of characteristic domains and on the mechanism of ubiquitin transfer to the substrate protein.[9] Because they mediate substrate specificity and generally exhibit remarkable plasticity, E3 ubiquitin ligases are the most frequently exploited component in proteome editing strategies described to date. For example, chemical knockdown has been achieved using small molecules called proteolysis targeting chimeras, or PROTACs,[10,11] which are hetero-bifunctional molecules containing one ligand for an E3 ubiquitin ligase, another ligand for the protein to be degraded, and a linker connecting the two. These molecules bind to both the E3 and the target, promoting the formation of a ternary complex that triggers target polyubiquitination followed by its proteasomal degradation. A growing number of peptide- and small-molecule-based PROTACs have been reported that enable chemical knockout in cells and in mice.[12−16] An attractive feature of these compounds is their drug-like properties including cell permeability; however, many peptide- and small-molecule-based PROTACs suffer from low potency—often requiring concentrations up to 25 μM to induce sufficient degradation[17]—and the generation of custom PROTACs is limited by the relative lack of available ligands for both E3 ubiquitin ligases and desired protein targets as well as the technical challenges associated with creating such ligands de novo.[18]

To circumvent these issues, our group and others have developed protein-based chimeras whereby E3 ubiquitin ligases are genetically fused to a protein that binds the target of interest. Following ectopic expression in cells, the engineered protein chimera recruits the E3 to the target protein, leading to its polyubiquitination and subsequent degradation by the proteasome. In the earliest example, protein knockout was achieved by creating an F-box chimera in which β-TrCP was fused to a peptide derived from the E7 protein encoded by human papillomavirus type 16 that is known to interact with retinoblastoma protein pRB.[19,20] Following ectopic expression, the engineered F-box recruited pRB to the Skp1-Cul1-F-box (SCF) machinery, a multiprotein E3 complex from the cullin-RING ligase (CRL) superfamily, for ubiquitination and destruction. A handful of other studies have similarly leveraged natural protein−protein interactions, whereby fusion of one interacting protein to an E3 yielded a chimera that silenced the corresponding binding partner following expression in cells and mice.[21−24]

More recently, we reported a universal proteome editing technology that could be extended beyond naturally occurring binding pairs. This approach involved fusing an E3 to a synthetic binding protein such as a single-chain antibody fragment (scFv), a designed ankyrin repeat protein (DARPin), or a fibronectin type III (*FN3*) monobody.[25] These bifunctional chimeras, called "ubiquibodies" (uAbs), combined the flexible ubiquitin-tagging capacity of the human RING/U-box-type E3 CHIP (carboxyl-terminus of Hsc70-interacting protein) with the engineerable affinity and specificity of synthetic binding proteins. The result is a customizable technology for efficiently directing otherwise stable proteins to the UPP for degradation independent of their biological function or interactions. Indeed, one of the greatest advantages of uAbs is their highly modular architecture—simply swapping synthetic binding proteins can generate a new uAb that specifically targets a different substrate protein,[26−30] while swapping E3 domains can alter the kinetics or mechanism of ubiquitin transfer. Moreover, by incorporating synthetic binding proteins that recognize particular protein states (e.g., active vs inactive conformation, mutant vs wild-type, post-translationally modified), it becomes possible to deplete certain protein subpopulations while sparing others.[20,31] At present, however, the development of uAbs has centered around a relatively narrow set of mammalian E3s, most notably the "stand alone" E3 CHIP or members of the CRL superfamily of multiprotein E3 ligase complexes. It remains unclear whether other candidates from the exceptionally large pool of naturally occurring E3 ligases might function as even more potent degraders in the uAb context.

Here, we attempted to broaden the range of E3s that can be functionally reprogrammed as bifunctional uAb chimeras. However, in a notable departure from previous efforts involving mammalian E3s, we focused instead on a set of effector proteins from microbial pathogens that mimic host E3 ubiquitin ligases and hijack the UPP machinery to dampen the innate immune response during infection.[32,33] The intrinsic plasticity of these enzymes led us to hypothesize that bacterial E3s could be manipulated for targeted proteolysis just like their mammalian counterparts. Indeed, robust target silencing was achieved with a uAb comprised of the *Shigella flexneri* E3 ligase IpaH9.8, which exhibits similarities to eukaryotic HECT-type E3s but is classified as a novel E3 ligase (NEL) due to the absence of sequence and structural homology with any eukaryotic E3s.[32−36] When the C-terminal catalytic NEL domain of IpaH9.8 was fused to the GFP-specific *FN3* monobody GS2 that specifically recognizes green fluorescent protein (GFP), we observed potent degradation of EGFP following both transient and stable expression in cultured mammalian cells. Moreover, the GS2-IpaH9.8 chimera was also able to accelerate the degradation of spectral derivatives of EGFP including Emerald, Venus, and Cerulean as well as 15 different FP-tagged mammalian proteins that ranged in size from 27 up to 179 kDa and localized in different subcellular

DOI: 10.1021/acscentsci.9b00127
ACS Cent. Sci. 2019, 5, 852−866

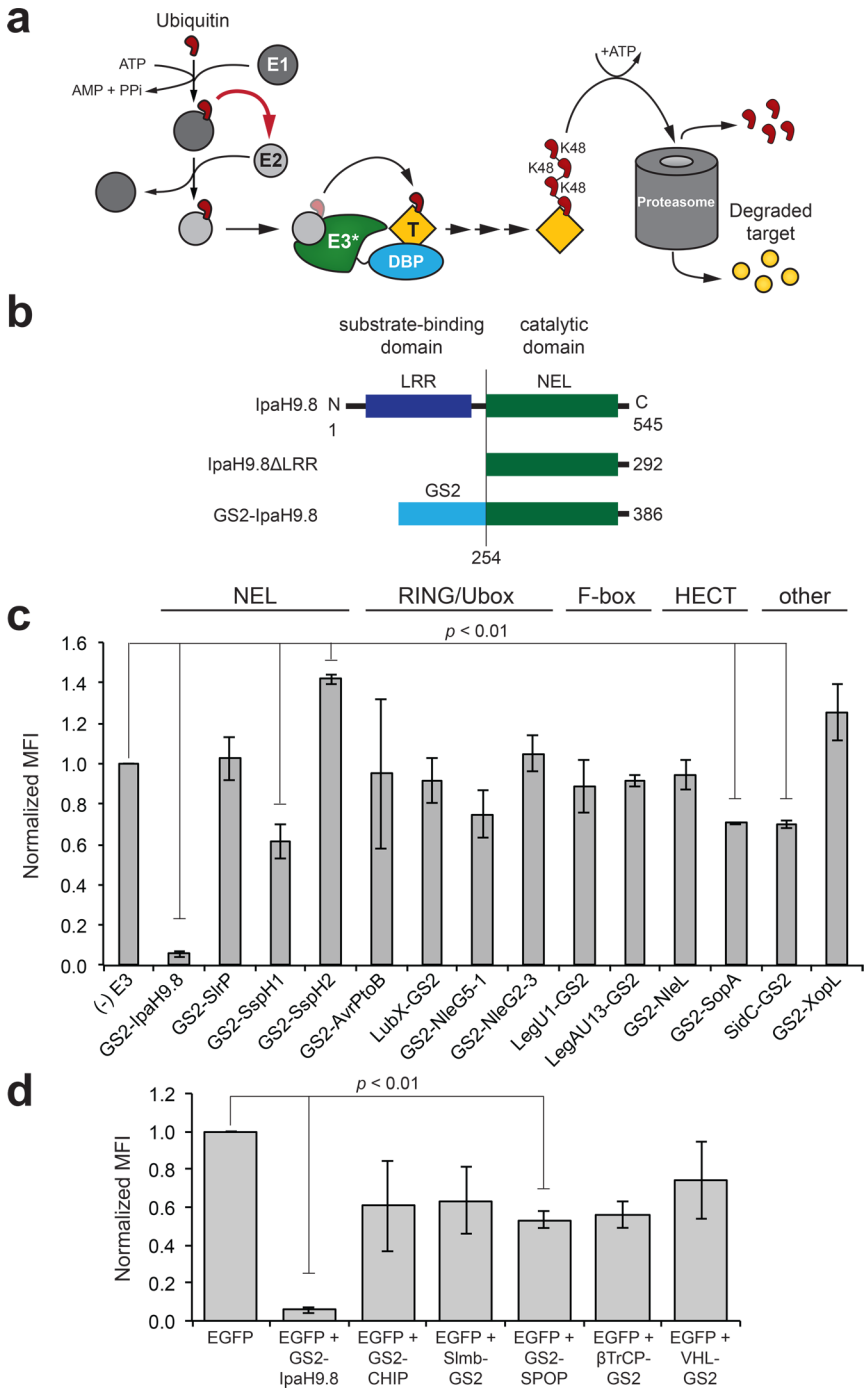

Figure 1. Engineering bacterial E3 ligase IpaH9.8 as a GFP-specific ubiquibody. (a) Schematic representation of ubiquibodies, chimeric fusions comprised of an E3 ubiquitin ligase catalytic domain (E3*) and a designer binding protein (DBP) that hijack the mammalian ubiquitin-proteasome pathway for degradation of desired protein targets (T). (b) Linear representation of IpaH9.8, IpaH9.8ΔLRR, and GS2-IpaH9.8. Numbers refer to amino acid positions from N-terminus (N) to C-terminus (C). The proteins are aligned vertically with the LRR and NEL domains of IpaH9.8. IpaH9.8ΔLRR is a truncated version of IpaH9.8 lacking the LRR domain. (c) Flow cytometric analysis of EGFP fluorescence activity in HEK293T cells transfected with plasmid pcDNA3-EGFP alone or cotransfected with pcDNA3-EGFP and a plasmid encoding one of the bacterial E3-based uAbs as indicated. (d) Same as in (c) but with mammalian E3-based uAbs as indicated. Data are biological triplicates (three separately transfected wells) of the geometric mean fluorescence intensity (MFI) normalized to MFI measured for HEK293T cells expressing EGFP alone. Error bars represent standard deviation (SD) of the mean. *p* values were determined by paired sample *t*-test.

compartments including the cytoplasm, nucleus, and cell membrane. For two of these targets, SHP2 and Ras, efficient silencing was also achieved when IpaH9.8 was fused to SHP2- or Ras-specific FN3 domains, highlighting the ease with which IpaH-based uAbs can be reconfigured.

As was noted previously, a major obstacle for the therapeutic development of uAbs is intracellular delivery.[18] Unlike smaller PROTACs, which can be designed for cell permeability,[17] uAbs are relatively bulky proteins that do not effectively penetrate the cell membrane. To remedy this issue, we implemented a bioinspired mRNA delivery strategy whereby

DOI: 10.1021/acscentsci.9b00127
ACS Cent. Sci. 2019, 5, 852−866

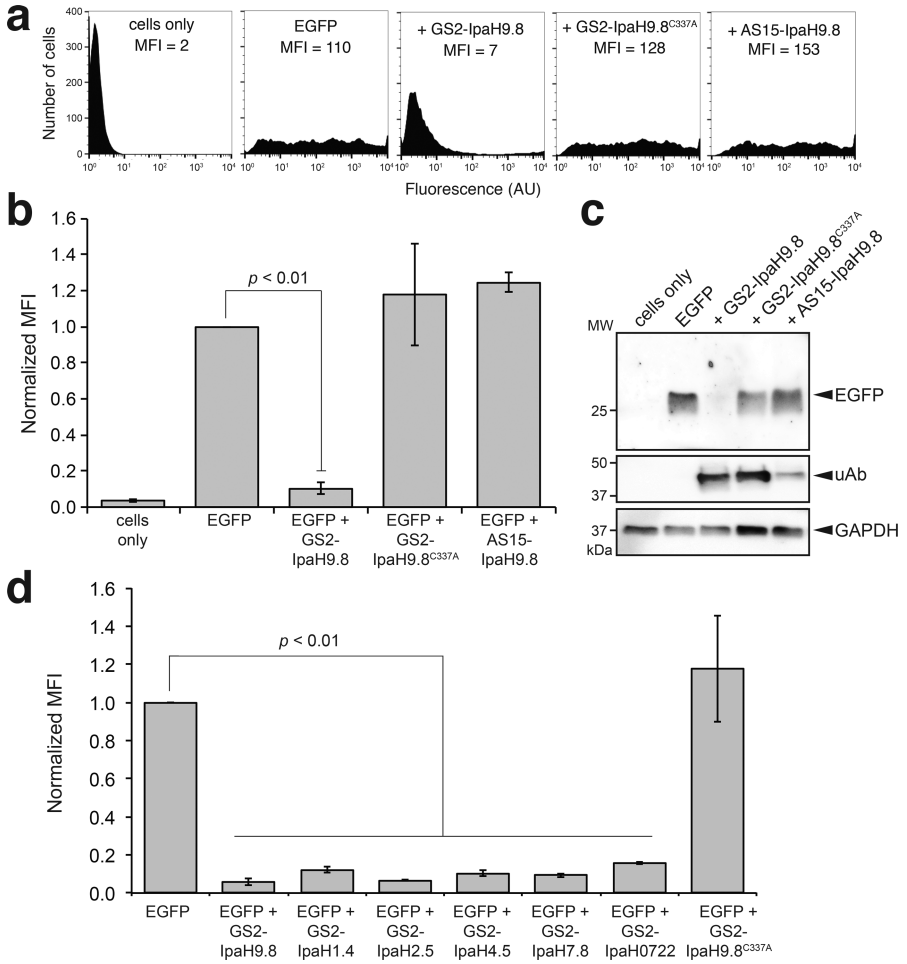

Figure 2. Catalytic domain of IpaH9.8 essential for ubiquibody function. (a) Representative fluorescence histograms obtained by flow cytometric analysis of EGFP fluorescence activity in HEK293T cells transfected with pcDNA3-EGFP alone or cotransfected with pcDNA3-EGFP and a plasmid encoding one of the following: GS2-IpaH9.8^{C337A}, AS15-IpaH9.8, or GS2-IpaH9.8. (b) Flow cytometric quantification of EGFP fluorescence activity for cells described in (a) where data are biological triplicates (three separately transfected wells) of the geometric MFI normalized to MFI measured for HEK293T cells expressing EGFP alone. Error bars represent standard deviation (SD) of the mean. (c) Western blot analysis of HEK293T cell lysates transfected as in (a) and (b). Blots were probed with antibodies specific for GFP, 6x-His (that detected tag on each uAb), and GAPDH as indicated. An equivalent amount of total protein was loaded in each lane as confirmed by immunoblotting with anti-GAPDH. Molecular weight (MW) markers are indicated on left. (d) Flow cytometric quantification of EGFP fluorescence activity for HEK293T cells cotransfected with pcDNA3-EGFP and a plasmid encoding GS2 fused to one of the IpaH9.8 homologues as indicated. Data are biological triplicates (three separately transfected wells) of the geometric MFI normalized to MFI measured for HEK293T cells expressing EGFP alone. Error bars represent standard deviation (SD) of the mean. *p* values were determined by paired sample *t*-test.

mRNA encoding GS2-IpaH with an additional 3′-terminal polyadenosine (poly A) tail was stoichiometrically complexed with poly A binding proteins (PABPs), which served to improve mRNA stability and also stimulate mRNA translation in eukaryotic cells.[37] The resulting ribonucleoproteins (RNPs) were stabilized with cationic polypeptides to protect the mRNA from degradation, enable its uptake by cells, and facilitate its endosomal escape. Importantly, these coassembled nanoplexes delivered GS2-IpaH9.8 mRNA in a manner that caused efficient GFP silencing after introduction to cultured mammalian cells stably expressing GFP and after administration to transgenic mice expressing GFP ubiquitously. Collectively, our results demonstrate that uAb-mediated proteome editing is an effective strategy for targeted degradation of proteins in cells and mice, thereby setting the stage for uAbs as tools for drug discovery and as therapeutic candidates with potential to pharmacologically hit so-called "undruggable" targets.

RESULTS

Engineered IpaH9.8 Potently Silences GFP in Mammalian Cells. To determine whether E3 ubiquitin ligase mimics from pathogenic bacteria could be redesigned for silencing of non-native targets, we focused on a panel of 14 candidate enzymes representing the major classes of E3s found in bacteria to date (Supplementary Table 1).[32,33] This panel included E3 mimics with folds similar to eukaryotic E3s such as HECT-type, RING or U-box (RING/U-box)-type, and F-box domains, as well as unconventional E3s with folds unlike any other eukaryotic E3s such as NEL, XL-box-containing, and SidC. In general, uAbs were engineered by removing the native substrate-binding domain from each E3 mimic and replacing it with a synthetic binding protein (Figure 1a), akin to our previously designed uAbs based on human CHIP.[25] For example, *S. flexneri* IpaH9.8 consists of an N-terminal domain with eight 20-residue leucine-rich repeats (LRRs) that mediate binding and specificity to native substrate proteins such as NF-

DOI: 10.1021/acscentsci.9b00127
ACS Cent. Sci. 2019, 5, 852−866

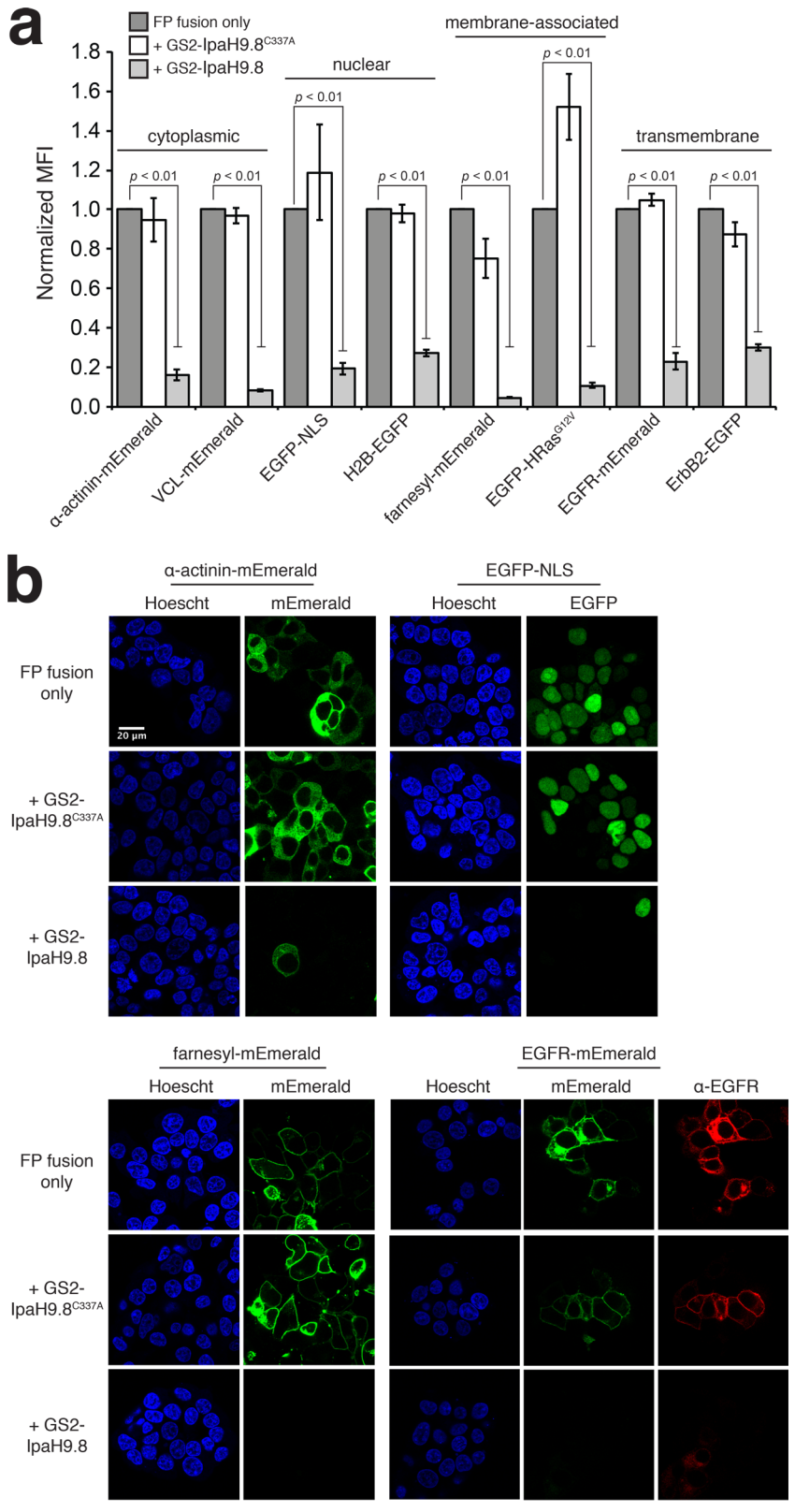

Figure 3. GS2-IpaH9.8 degrades structurally diverse fluorescent protein fusions. (a) Flow cytometric quantification of fluorescence activity in HEK293T cells transfected with a plasmid encoding the indicated FP fusion alone (dark gray) or cotransfected with the FP fusion plasmid and either pcDNA3-GS2-IpaH9.8^{C337A}(white) or pcDNA3-GS2-IpaH9.8 (light gray). Data are biological triplicates (three separately transfected wells) of the geometric MFI normalized to MFI measured for HEK293T cells expressing the corresponding FP fusion protein alone. Error bars represent standard deviation (SD) of the mean. (b) Confocal microscopy images corresponding to select FP targets expressed in HEK293T cells transfected/cotransfected as described in (a). Hoescht stain (blue) denotes cell nuclei, and EGFP signal (green) denotes fluorescent proteins. For the EGFR-mEmerald fusion, immunostaining with an EGFR-specific antibody (red) is also depicted. *, $p < 0.01$ as determined by paired sample *t*-test.

DOI: 10.1021/acscentsci.9b00127
ACS Cent. Sci. 2019, 5, 852−866

κB essential modulator (NEMO)[38] and guanylate-binding proteins (GBPs),[39] while the C-terminal domain adopts a novel E3 ubiquitin ligase architecture.[34,35] Hence, we replaced the N-terminal LRR domain of IpaH9.8 with GS2, an FN3 monobody that binds GFP with nanomolar affinity (K_d = 31 nM).[40] By swapping the natural substrate recognition function of these enzymes with the GS2 monobody, synthetic E3 ligases were created that we hypothesized would target GFP and promote its proteasomal degradation. To test this hypothesis, the different GS2−E3 chimeras were transiently coexpressed along with enhanced GFP (EGFP) in mammalian cells, and fluorescence activity was monitored by flow cytometric analysis. By far, the most striking depletion of EGFP was achieved with GS2-IpaH9.8, which reduced EGFP fluorescence to near background levels (Figure 1b and Supplementary Figure 1). All of the other uAbs showed relatively weak silencing activity under the conditions tested here. GS2-NleG5-1, GS2-SspH1, SidC-GS2, and GS2-SopA were the most active among these, reducing EGFP fluorescence by ∼20−40% (Figure 1b and Supplementary Figure 1).

In light of this robust silencing activity, we decided to focus our attention on the GS2-IpaH9.8. In cells expressing this chimera, the elimination of EGFP was efficient, with removal of up to 90% of the fluorescence activity (Figure 2a,b) and no detectable EGFP protein in cell lysates (Figure 2c). Importantly, silencing activity was completely abrogated when the catalytic cysteine of IpaH9.8[36] was mutated to alanine (GS2-IpaH9.8^{C337A}) and when the noncognate FN3 monobody AS15, which is specific for the Abl SH2 domain,[41] was substituted for GS2 (Figure 2a−c), indicating that target degradation was dependent on cooperation of both uAb domains. In the case of GS2-IpaH9.8^{C337A}, expression in mammalian cells and EGFP-binding activity in vitro were unaffected by the alanine substitution (Supplementary Figure 2), confirming that loss of silencing activity was due to catalytic inactivation. It should also be noted that removal of the LRR domain was essential for knockdown activity, as direct fusion of GS2 to full-length IpaH9.8 that had not been truncated resulted in no measurable silencing activity (data not shown). Interestingly, the genome sequences of *S. flexneri* strains indicate that several IpaH family members, namely, IpaH1.4, IpaH2.5, IpaH4.5, IpaH7.8, and IpaH9.8, are encoded on the 220-kb virulence plasmid pWR100, while seven additional *ipaH* cognate genes are present on the chromosome.[32] To determine whether these family members were as proficient as IpaH9.8 at degrading EGFP in the uAb context, we generated chimeras between GS2 and the catalytic domains derived from each of the pWR100-encoded IpaH family members as well as one chromosomally encoded member, IpaH0722. When expressed ectopically in cultured cells, all of the IpaH-based uAbs were capable of efficient (∼90% or greater) EGFP knockdown in mammalian cells (Figure 2e). This result was not entirely surprising in light of the high homology shared by the different catalytic domains. Indeed, whereas the different IpaH family members were only ∼70% similar to IpaH9.8 overall, the catalytic domains were much more similar (>99%) with just 1−3 amino acid substitutions and, in the case of IpaH1.4 and IpaH4.5, minor C-terminal truncations (Supplementary Table 1).

To benchmark the potency of our engineered bacterial ligase, we compared the GFP silencing activity catalyzed by GS2-IpaH9.8 with that of other synthetic ligases based on eukaryotic E3 machinery that have previously been reconfigured for targeted proteolysis.[19−23,26−30] Specifically, the natural substrate-binding domains for several eukaryotic E3 ubiquitin ligases from humans including carboxyl-terminus of Hsc70-interacting protein (CHIP), speckle-type POZ protein (SPOP), β-transducing repeat-containing protein (βTrCP), and von Hippel-Lindau protein (VHL), as well as the *Drosophila melanogaster* supernumerary limbs (Slmb) protein were replaced with the GS2 monobody, resulting in a panel of synthetic ligases analogous to GS2-IpaH9.8. When the resulting panel of GFP-specific uAbs was transiently coexpressed with EGFP in mammalian cells, all were capable of measurably reducing EGFP levels, but silencing activity for each was relatively inefficient (∼25−45%) under the conditions tested here (Figure 1c and Supplementary Figure 1), reminiscent of previous results with a Slmb-nanobody chimera that was similarly ineffective at reducing unfused GFP levels.[26] The weak EGFP knockdown observed here for Slmb-GS2 was actually an improvement over previous results obtained with a chimera between Slmb and a GFP-specific VHH nanobody, cAbGFP4, that was incapable of promoting degradation of unfused GFP.[26] It should be noted, however, that the Slmb-cAbGFP4 fusion eliminated the fluorescence associated with larger GFP fusion proteins, suggesting that the data reported here are not necessarily indicative of uAb dysfunction but instead may reflect differences in substrate preference/compatibility or extent of ubiquitin decoration. Regardless, none of the engineered chimeras involving eukaryotic E3s displayed the potency and robustness of GS2-IpaH9.8, which reproducibly degraded 90−95% of cellular fluorescence.

A Broad Range of Substrate Proteins Is Degraded by GS2-IpaH9.8. To more deeply explore the substrate compatibility issue, we tested the ability of GS2-IpaH9.8 to degrade a range of different substrates. A growing number of GFP-derived fluorescent proteins (FPs) have been developed and optimized over the years, providing a diverse collection of new tools for biological imaging.[42,43] To determine the extent to which different FP targets could be degraded, GS2-IpaH9.8 was transiently coexpressed in mammalian cells with monomeric versions of Emerald, Venus, and Cerulean, as well as enhanced cyan fluorescent protein (ECFP). Approximately 65−85% of the cellular fluorescence activity associated with each of the FPs was ablated by GS2-IpaH9.8, whereas the structurally unrelated mCherry protein was not targeted by GS2-IpaH9.8, which was expected given the specificity of GS2 for the GFP fold (Supplementary Figure 3a). Interestingly, the fluorescence activity of superfolder GFP (sfGFP), a rapidly folding and robustly stable mutant of EGFP, was unaffected by GS2-IpaH9.8, consistent with recent findings that sfGFP is resistant to proteasomal degradation.[44]

Encouraged by the ability of GS2-IpaH9.8 to degrade different FPs, we next evaluated the ability of GS2-IpaH9.8 to degrade structurally diverse, FP-tagged substrate proteins. GS2-IpaH9.8 proficiently degraded 15 unique target proteins that varied in terms of their molecular weight (27−179 kDa) and subcellular localization (i.e., cytoplasm, nucleus, membrane-associated, and transmembrane) (Figure 3a and Supplementary Figure 3b). For example, GS2-IpaH9.8 triggered degradation of 80−92% of the fluorescence activity associated with FP fusions involving the cytoplasmic proteins α-actinin, α-synuclein (α-syn), extracellular signal-regulated kinase 2 (ERK2), focal adhesion kinase (FAK), F-tractin, paxillin (PXN), and vinculin (VCL) as determined by flow

DOI: 10.1021/acscentsci.9b00127
ACS Cent. Sci. 2019, 5, 852−866

cytometric analysis (Figure 3a and Supplementary Figure 3b). Similarly robust silencing was observed for nuclear-targeted FP fusions involving histone H2B and the nuclear localization signal (NLS) derived from SV40 Large T-antigen, membrane-associated FP fusions involving Harvey rat sarcoma virus oncogene homologue carrying the oncogenic G12V mutation ($HRas^{G12V}$), Src-homology 2 domain-containing phosphatase 2 (SHP2), and the farnesyl sequence derived from HRas, and transmembrane FP fusions involving epidermal growth factor receptor (EGFR), avian erythroblastic leukemia viral oncogene homologue 2 (ErbB2), and mucin 1 (MUC1) (Figure 3a and Supplementary Figure 3b). Microscopy analysis of representative substrate proteins α-actinin-mEmerald, EGFP-NLS, farnesyl-mEmerald, and EGFR-mEmerald confirmed the expected subcellular localization of each fusion and corroborated the efficient degradation activity measured by flow cytometric analysis (Figure 3b). The transmembrane protein EGFR-mEmerald was examined by immunolabeling with an antibody specific to the extracellular domain of EGFR. Importantly, the α-EGFR signal decreased concomitantly with GFP disappearance (Figure 3b), indicating that degradation of the entire transmembrane protein was achieved. Taken together, these results establish GS2-IpaH9.8 as a robust proteome editing tool that is capable of silencing a broad spectrum of substrates that span several distinct subcellular locations.

GS2-IpaH9.8-Mediated Proteome Editing Is Flexible and Modular. An attractive feature of uAbs is their highly modular architecture—the E3 catalytic domain and synthetic binding protein domain can be interchanged to reprogram the activity and specificity. Indeed, our results above revealed the ease with which different bacterial and eukaryotic E3 domains can be chimerized to form functional uAbs. To investigate the interchangeability of the synthetic binding protein domain in IpaH9.8-based uAbs, we first replaced GS2 with other high-affinity GFP-binding proteins such as the FN3 monobody GS5 (K_d = 62 nM)[40] or cAbGFP4 (K_d = 0.32 nM).[45] For these constructs, efficient EGFP silencing activity was observed that rivaled that seen with the GS2 monobody (Supplementary Figure 4a). Interestingly, introduction of weaker affinity (~200−500 nM) FN3 monobodies[40] resulted in less efficient EGFP elimination (Supplementary Figure 4a), suggesting that silencing activity may be a function of the affinity for the target protein. However, because spatial arrangements and surface complementarity prioritize lysine sites for ubiquitination,[9] an equally plausible explanation for these findings is that the various FN3 domains may differentially orient the uAb with respect to GFP in a manner that affects how the substrate is ubiquitinated.

We next investigated the compatibility of the IpaH9.8 catalytic domain with two different FN3 monobodies: NSa5 that is specific for the Src-homology 2 (SH2) domain of SHP2[46] and RasInII that is specific for HRas, KRas, and the G12V mutants of each.[47] The resulting NSa5-IpaH9.8 and RasInII-IpaH9.8 chimeras were tested for their ability to silence SHP2-EGFP and EGFP-$HRas^{G12V}$, respectively, by flow cytometric analysis. Both exhibited strong silencing activity, degrading their EGFP-tagged targets almost as efficiently as the GFP-directed GS2-IpaH9.8 (Figure 4a,b). Interestingly, RasInII-IpaH9.8 degraded EGFP-$KRas^{G12C}$ and other KRas mutants (e.g., G12D, G12V) more efficiently than EGFP-KRas (Figure 4c), in line with its selectivity for the G12V mutant over wild-type Ras isoforms[47] and thus providing a potential route for mutant selective silencing of Ras. Collectively, these results reveal a remarkable plasticity for IpaH9.8, enabling its

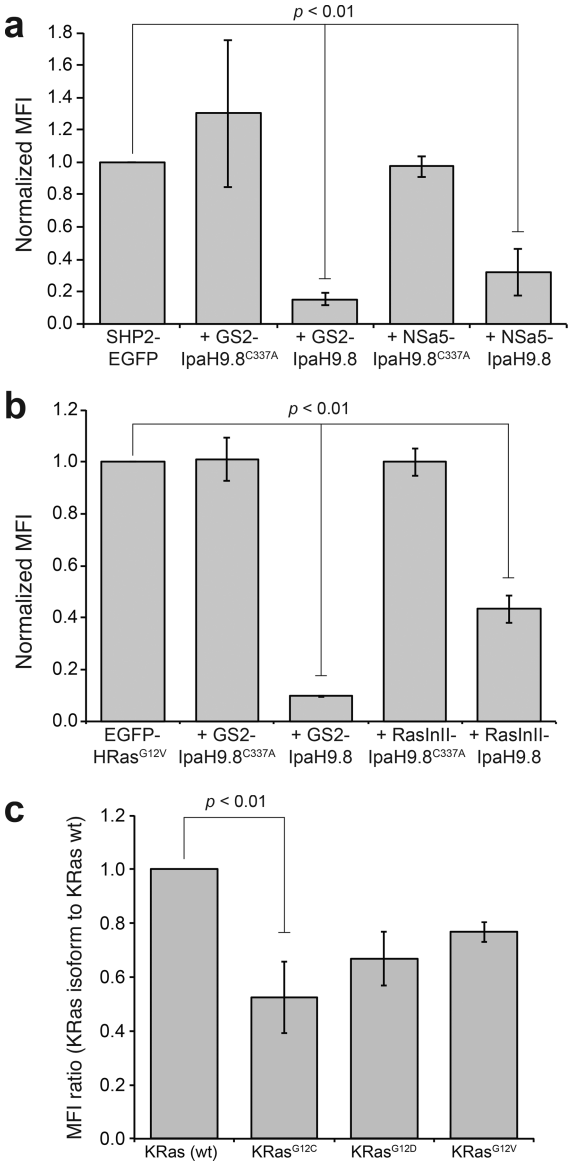

Figure 4. IpaH9.8 ubiquibodies directed against disease-relevant targets. (a) Flow cytometric quantification of EGFP fluorescence activity in HEK293T cells transfected with pcDNA3-SHP2-EGFP alone or cotransfected with pcDNA3-SHP2-EGFP and a plasmid encoding one of the following: GS2-IpaH9.8, GS2-$IpaH9.8^{C337A}$, NSa5-IpaH9.8, or NSa5-$IpaH9.8^{C337A}$. (b) Same as in (a) but with pcDNA3-EGFP-$HRas^{G12V}$ alone or cotransfected with pcDNA3-EGFP-$HRas^{G12V}$ and a plasmid encoding one of the following: GS2-IpaH9.8, GS2-$IpaH9.8^{C337A}$, RasInII-IpaH9.8, or RasInII-$IpaH9.8^{C337A}$. Data are biological triplicates (three separately transfected wells) of the geometric MFI normalized to MFI measured for HEK293T cells expressing EGFP alone. Error bars represent standard deviation (SD) of the mean. (c) Flow cytometric quantification of EGFP fluorescence activity in HEK293T cells cotransfected with pcDNA3-RasInII-IpaH9.8 and one of the following: pcDNA3-EGFP-KRas, pcDNA3-EGFP-$KRas^{G12C}$, pcDNA3-EGFP-$KRas^{G12D}$, or pcDNA3-EGFP-$KRas^{G12V}$. MFI ratio was determined by normalizing geometric MFI for cells expressing KRas mutant to geometric MFI for cells expressing wild-type (wt) KRas. Data are the average of biological triplicates (three separately transfected wells), and error bars represent standard deviation (SD) of the mean. p values were determined by paired sample t-test.

DOI: 10.1021/acscentsci.9b00127
ACS Cent. Sci. 2019, 5, 852−866

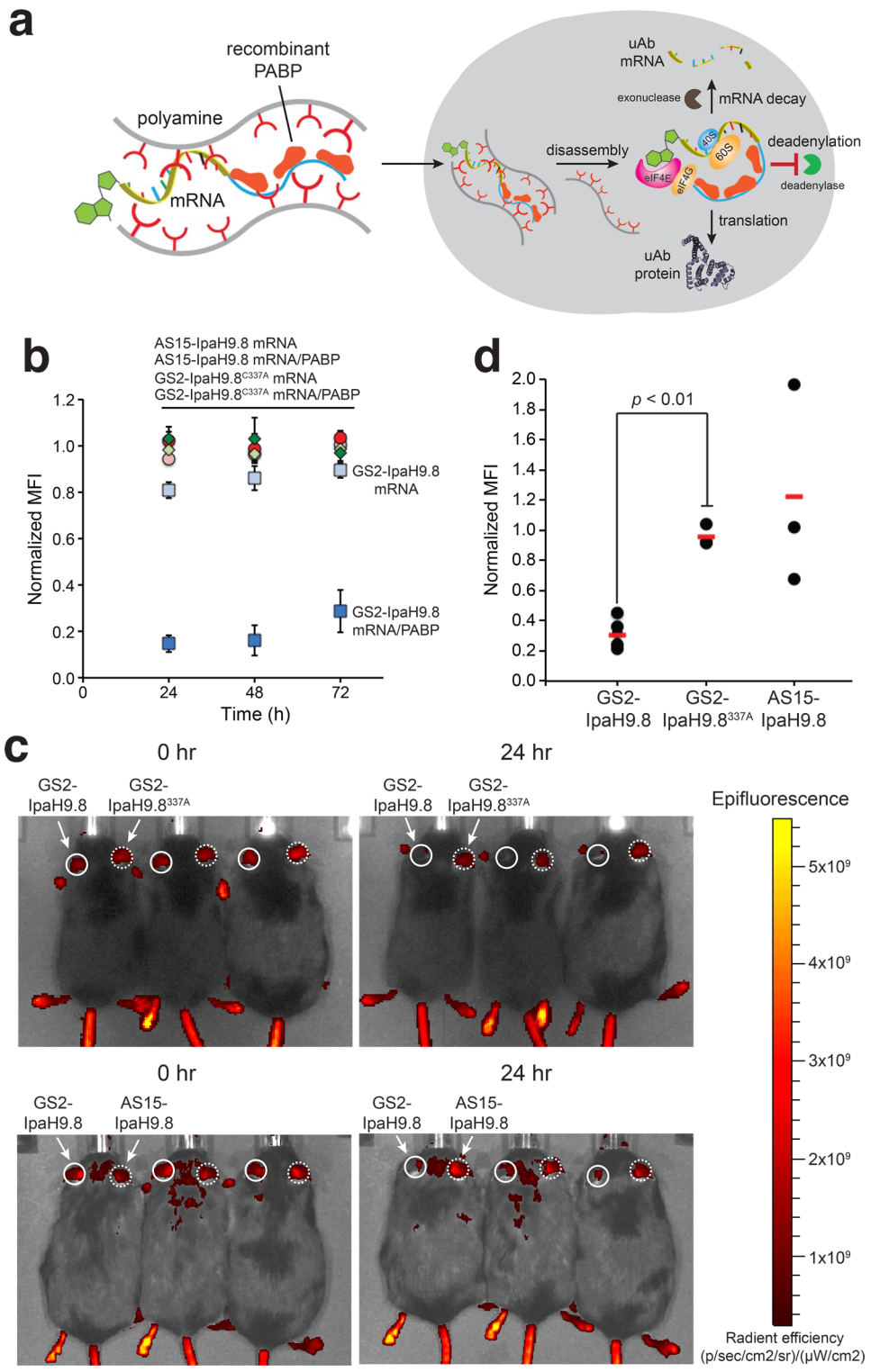

Figure 5. Proteome editing in mice via nanoplex delivery of ubiquibody mRNA. (a) Schematic of polyamine (TEP (N4))-mediated stoichiometric assembly of mRNA/PABP ribonucleoproteins for enhanced mRNA delivery (see text for details). Following internalization in cells (gray circle), nanoplex disassembly results in the release of mRNA/PABP that is either degraded or translated to produce uAb proteins. (b) Flow cytometric quantification of EGFP fluorescence activity in HEK293Td2EGFP cells incubated with mRNA encoding GS2-IpaH9.8, GS2-IpaH9.8^{C337A}, or AS15-IpaH9.8; or with nanoplexes comprised of the same mRNAs formulated with PABP and TEP (N4) polyamine (mRNA:PABP weight ratio = 1:5). Measurements were taken at 24, 48, and 72 h post delivery. Data are expressed as the mean ± SD of biological triplicates (three separately treated wells). (c) Epifluorescence imaging of UBC-GFP mice at 0 h (top) and 24 h (bottom) after ear injection of nanoplexes containing mRNA encoding GS2-IpaH9.8 (solid white circle), GS2-IpaH9.8^{C337A} (dashed white circle, top), or AS15-IpaH9.8 (dashed white circle, bottom). Numbers on the heat bar represent radiant efficiency (p/sec/cm^2/sr)/(μW/cm^2) (d) Quantification of GFP fluorescence in the ears of Ubi-GFP mice in (c). Data are reported as the mean radiant efficiency for each individual ear region (black circle) and the mean radiant efficiency (red bar) of each sample group (n = 6 for GS2-IpaH9.8, n = 3 for GS2-IpaH9.8^{C337A}, and n = 3 for AS15-IpaH9.8). p values were determined by paired sample t-test.

DOI: 10.1021/acscentsci.9b00127
ACS Cent. Sci. 2019, 5, 852−866

use as a "one size fits all" degrader of diverse target proteins in transiently and stably transfected cell lines.

In all the experiments described above, efficient knockdown was achieved when GS2-IpaH9.8 and its corresponding target were transiently expressed. However, transient expression is not always an option, due to the experimental time scale, necessity for a precise expression profile, or the use of a recalcitrant mammalian cell line. Thus, to demonstrate the flexibility of GS2-IpaH9.8-mediated silencing, we evaluated degradation activity against target proteins that were expressed as stably integrated transgenes. Specifically, when GS2-IpaH9.8 was transiently expressed in cells that stably coexpressed EGFP, reduction of fluorescence activity was virtually identical to that observed for transiently expressed EGFP (Supplementary Figure 4b). Robust degradation was also observed for ERK2-EGFP, H2B-EGFP, and EGFP-HRas^{G12V}, regardless of their mode of expression (Supplementary Figure 4b). When the uAb and the target were both expressed as stable transgenes, thereby eliminating the need for transfection entirely, strong silencing activity was again observed for GS2-IpaH9.8 but not its inactive GS2-IpaH9.8^{C337A} counterpart (Supplementary Figure 4c).

Delivery of mRNA Encoding GS2-IpaH9.8 Enables Proteome Editing in Mice. From a therapeutic standpoint, one of the biggest challenges facing protein-based technologies such as uAbs is intracellular delivery.[18] We previously showed that coassembled nanoplexes comprised of synthetic mRNA containing a poly A tail, PABPs, and biocompatible cationic polypeptides (Figure 5a) resulted in greatly enhanced mRNA expression in vitro and in mice.[37] Here, we hypothesized that delivery of GS2-IpaH9.8 mRNA/PABP nanoplexes to mammalian cells would result in significantly greater uAb expression relative to mRNA transfection alone by the same polyamine in HEK293T cells, thereby leading to potent protein degradation. To test this hypothesis, we first evaluated GS2-IpaH9.8 mRNA/PABP nanoplex delivery in vitro by quantifying the degradation of d2EGFP, a destabilized GFP variant that was expressed as a stable transgene in HEK293T cells. As expected, only when the cationic nanoplexes contained the active, target-specific GS2-IpaH9.8 mRNA and PABP was robust d2EGFP degradation achieved (Figure 5b). All other controls including catalytically inactive GS2-IpaH9.8^{C337A} mRNA/PABP nanoplexes, nonspecific AS15-IpaH9.8 nanoplexes, and naked GS2-IpaH9.8 mRNA that was delivered without PABPs showed little to no silencing activity (Figure 5b). At 24 h post-treatment, HEK293Td2EGFP cells receiving GS2-IpaH9.8 mRNA/PABP nanoplexes exhibited an 85% decrease in fluorescence activity, which was directly comparable to the knockdown activity achieved following DNA transfection seen above.

Encouraged by these results, we next evaluated uAb nanoplex-mediated delivery and silencing activity in vivo. Transgenic UBI-GFP/BL6 mice, which constitutively express EGFP in all tissues,[48] were given subcutaneous injections of GS2-IpaH9.8 mRNA/PABP nanoplexes in ears. Note that although this mouse strain ubiquitously expresses EGFP, fluorescence is absorbed and undetectable in areas that are covered by hairs. Fluorescent imaging at 24 h postinjection revealed that EGFP fluorescence in the left ears, which received GS2-IpaH9.8 mRNA/PABP nanoplex injections, was robustly ablated with a 70% decrease in ear fluorescence (Figure 5c,d). In stark contrast, fluorescence in the right ears, which received either catalytically inactive GS2-IpaH9.8^{C337A} or nonspecific AS15-IpaH9.8 nanoplex injections, was unaffected (Figure 5c,d). Importantly, these results set the stage for therapeutic delivery of uAbs as a viable strategy to post-translationally silence aberrantly expressed proteins in cancer and other human diseases.

DISCUSSION

Ubiquibodies are a relatively new proteome editing modality that enable selective removal of otherwise stable proteins in somatic cells,[25] with potential applications in basic research, drug discovery, and therapy. In this study, we created a new class of uAbs that feature bacterial E3 ubiquitin ligases, thereby opening the door to a previously untapped source of ubiquitination activity for uAb development. Specifically, we evaluated 14 bacterial E3 ligases belonging to a growing class of effector proteins that mimic host cell E3 ligases to exploit the ubiquitination pathway.[32,33] Most notable among these was IpaH9.8 from *S. flexneri*, which proved to be a remarkable catalyst of protein turnover when directed to target substrates via a genetically fused synthetic binding domain. This silencing activity was found to be independent of the substrate's subcellular localization (i.e., cytoplasm, nucleus, plasma membrane) or expression modality (i.e., transient versus stable). The only other E3 ligases that functioned comparably were homologues of IpaH9.8 found in *S. flexneri*, either on the pWR100 virulence plasmid or the chromosome.[32] The N-terminal catalytic NEL domains of these enzymes share striking homology (99−100%), which explains their similar performance in the uAb context. Accordingly, the next best functioning bacterial E3 ubiquitin ligase was *S. typhimurium* SspH1, which is also a NEL type enzyme with 38% identity to IpaH9.8 overall and 42% identity within the NEL domain.[49] It should also be pointed out that none of the mammalian E3 ubiquitin ligases were able to degrade EGFP levels below 60% under the conditions tested here. While the reasons for this are not entirely clear, given the successful knockdown results reported previously for these different E3 ligases in the uAb format,[25−30] it is possible that EGFP may represent a poor substrate for these engineered chimeras. It is worth noting, however, that when each of the bacterial or mammalian E3-based uAbs was tested against a different substrate, namely, EGFP-HRas^{G12V}, very similar results were observed. That is, a handful (e.g., XopL, CHIP, SPOP, and βTrCP) were able to reduce EGFP-HRas^{G12V} levels by as much as 60%, but none were as effective as IpaH9.8 or its homologues, which all degraded ∼80−90% of EGFP-HRas^{G12V} (Supplementary Figure 5a−c).

While the work here was predominantly focused on silencing FPs and FP-tagged substrates, we also designed IpaH9.8-based uAbs that potently degraded disease-related targets including HRas, which together with KRas and NRas comprise the most commonly mutated oncoproteins in cancer, and SHP2, a regulator of the Ras/MAPK signaling pathway. Importantly, the ability to deplete these clinically important targets along with all of the other FP fusions serves to highlight the extraordinary modularity of the uAb technology. Simply swapping the native substrate-binding domain of the E3 ubiquitin ligase can generate a made-to-order uAb with specificity for a different substrate protein. Interestingly, *Shigella* have evolved a similar strategy for subverting host defenses during infection whereby plasmid and chromosomally encoded IpaH proteins play a key role in dampening the host inflammatory response by mediating proteasomal degradation

DOI: 10.1021/acscentsci.9b00127
ACS Cent. Sci. 2019, 5, 852−866

of NF-κB-related proteins.[38,50] Specifically, by employing different LRR domains, which only share ∼50% similarity,[49] *Shigella* are able to redirect virtually identical catalytic NEL domains to an array of host proteins (e.g., NEMO, U2AF53 for IpaH9.8; glomulin for IpaH7.8; p65 for IpaH4.5; HOIP for IpaH2.5 and IpaH1.4; TRAF2 for IpaH0722).[32,33,50] We believe that the inherent conformational flexibility required to ubiquitinate these structurally diverse substrates helps to explain the NEL motif's remarkable ability for customizable target degradation. It should also be pointed out that while the work here leveraged previously confirmed E3 ubiquitin ligases, an analogous swapping strategy could be used to create GS2-based uAbs for identifying novel E3 ligases. Such an approach could enable systematic identification of E3 ligases, which is an important objective given that the human genome encodes over 600 putative E3 ligases[51] and bacterial genomes likely encode hundreds of others, many of which remain to be validated as catalysts of ubiquitin transfer.

From a drug development standpoint, pharmacological control of gene products has traditionally been achieved using small molecule inhibitors that target enzymes and receptors having well-defined hydrophobic pockets where the small molecules are tightly bound. Unfortunately, a majority (∼80−85%) of the human proteome is comprised of intractable targets, such as transcription factors, scaffold proteins, and nonenzymatic proteins, that cannot be inhibited pharmacologically and thus have been deemed "undruggable".[52,53] As an alternative, a number of techniques for silencing proteins at the DNA or RNA level are now available such as CRISPR, RNAi, TALENs, and ZFNs, with the first RNAi therapy, patisiran, gaining approval in 2018 for hereditary transthyretin amyloidosis.[54] Nonetheless, new adaptable technologies, such as uAbs and the related PROTACs technology, that offer temporal and post-translational control over protein silencing are desirable especially because of their potential to overcome some of the limitations associated with nucleic acid targeting-based approaches such as irreversibility, lack of temporal control, and off-target effects.[2,4,55,56] In principle, both uAbs and PROTACs can degrade proteins regardless of their function, including the currently undruggable proteome. Moreover, unlike conventional "occupancy-based" therapeutics, uAbs and PROTACs act catalytically, making them substantially more potent than the target-binding antibody mimetics and small molecule inhibitors, respectively, from which they are built.

A major advantage of uAbs is the ease with which they can be rapidly adapted to hit a variety of intracellular targets due to their recombinant, modular design, which capitalizes on a large, preexisting repertoire of synthetic binding proteins as well as systematic, genome-wide efforts to generate and validate protein binders de novo against the human proteome.[57] Because obtaining antibody mimetics that bind with high specificity and affinity to a target should be easier than obtaining small molecules with the same properties, making custom-designed PROTACs is likely to be a much more challenging task.[18] Nonetheless, PROTACs holds great promise as a therapeutic approach because it is based on small molecules that have strong odds of getting into cells. Indeed, impressive preclinical in vitro and in vivo data are propelling the development of clinically viable PROTACs as evidenced by the founding of Arvinas in 2013 and C4 Therapeutics in 2016. It should be pointed out, however, that traditional medicinal chemistry approaches will be needed to improve the oral bioavailability, pharmacokinetics, and absorption, distribution, metabolism, excretion and toxicity (ADMET) properties of PROTACs.[10,11] Compared to PROTACs, intracellular delivery of uAb-based therapeutics is a much bigger hurdle as most globular protein drugs do not spontaneously cross plasma membranes due to their relatively large size and biochemical properties.[18] One possible solution that we investigated here is the use of mRNA as a source of therapeutic gene product in vivo. In recent years, impediments to the use of mRNA, including its instability and immunogenicity, have been largely overcome through structural modifications, while issues related to delivery and protein expression profiles have been addressed through advances in nanotechnology and material science.[58] Here, we take advantage of our unique approach to create a first-in-kind therapeutic uAb delivery strategy; this method involved a recently reported strategy of electrostatics to stabilize preformed protein−RNA complexes for delivery.[37] In terms of longevity of knockdown, this earlier study demonstrated that tail vein injection of nanoplexes formulated with luciferase mRNA resulted in the highest luciferase expression levels at 6 h postinjection, which remained statistically above control at 24 h postinjection but significantly decayed to background after 48 h. While this previous work did not involve uAbs directly, it does provide a sense for the longevity that might be possible using this delivery method. Here, synthetic mRNA encoding the GFP-directed GS2-IpaH9.8 chimera was coassembled with PABPs, and the assembled ribonucleoproteins were packaged into nanosized complexes using structurally defined polypeptides bearing cationic aminated side groups. The resulting nanoplexes achieved highly efficient silencing of GFP in vitro and in vivo, thereby demonstrating a new proteome editing paradigm and opening the door to clinical translation of uAb-based therapeutics.

EXPERIMENTAL METHODS

Plasmids. All plasmids used in this study are provided in Supplementary Table 2. *Escherichia coli* strain DH5α was used for the construction and propagation of all plasmids. To construct pcDNA3-EGFP, EGFP was PCR amplified using primers that introduced a 5′ Kozak sequence, and the resulting PCR product was ligated into pcDNA3. Plasmid pCDH1-ERK2-EGFP was created by gene assembly of ERK2 and EGFP using overlap extension PCR with primers that introduced a 5′ Kozak sequence followed by ligation into pCDH1. Plasmid pcDNA3-EGFP-NLS was created by PCR amplification of EGFP with primers that added a 5′ Kozak sequence and 3′ SV40 NLS sequence and then ligation of the PCR product into pcDNA3. Plasmid pcDNA3-SHP2-EGFP was created by PCR amplification of SHP2 with a 5′ Kozak sequence followed by ligation into pcDNA3-EGFP. Plasmid pcDNA3-EGFP-HRas^{G12V} was generated by PCR amplification of EGFP-HRas from plasmid mEGFP-HRas G12V, and the PCR product was subsequently ligated into pCDH1.

For creation of GFP-directed uAbs, plasmid pcDNA3-HF-GS2 was created by PCR amplification of GS2 from pHFT2-GS2[40] using primers that introduced upstream Kozak, 6x-His, and FLAG sequences followed by ligation into pcDNA3 such that *Bam*HI and *Eco*RI restriction sites were available upstream of GS2 for generating N-terminal fusions. For C-terminal fusions, plasmid pcDNA3-GS2-FH was created by PCR amplifying GS2 with primers that introduced an upstream Kozak sequence and downstream NheI and SbfI restriction

DOI: 10.1021/acscentsci.9b00127
ACS Cent. Sci. 2019, 5, 852−866

sites followed by ligation into pcDNA3. The genes encoding AvrPtoB, IpaH9.8, NleG2-3, NleG5-1, NleL, SlrP, SopA, SPOP, SspH1, SspH2, and XopL were PCR amplified with primers introducing NheI and SbfI sites, after which the resulting PCR products were ligated in pcDNA3-GS2-FH. The genes encoding LegAU13, LegU1, and SidC were PCR amplified with primers that introduced *Bam*HI and *Eco*RI sites, after which the resulting PCR products were ligated in pcDNA3-HF-GS2. Plasmid pcDNA3-GS2-CHIP was created by PCR amplification of GS2 from pHFT2-GS2 using primers that introduced an upstream *Hin*dIII and Kozak sequence and downstream NheI site, followed by ligation into pcDNA3-R4-CHIPΔTPR in place of scFvR4. Plasmids pcDNA3-VHL-GS2 and pcDNA3-βTrCP-GS2 were created by PCR amplification of genes encoding VHL and βTrCP with primers that introduced HindII and XhoI (VHL) or *Bam*HI and XhoI (βTrCP) sites after which the resulting PCR products were ligated in place of NSlmb in pcDNA3-NSlmb-GS2. Plasmids pcDNA3-GS2-IpaH9.8^{C337A}, pcDNA3-GS2-IpaH0722, pcDNA3-GS2-IpaH1.4, pcDNA3-GS2-IpaH2.5, pcDNA3-GS2-IpaH4.5, and pcDNA3-GS2-IpaH7.8 were created by site-directed mutagenesis of pcDNA3-GS2-IpaH9.8. The following genes were purchased: SspH1 (Twist Biosciences), IpaH9.8 (Twist Biosciences), VHL (GenScript, Ohu23297D), LubX (Twist Biosciences), LegU1(IDT), and LegAU13 (IDT). All others were amplified from existing plasmids in our laboratory stocks or from genomic DNA.

Plasmid pET24d-GS2-IpaH9.8 and pET24d-IpaH9.8ΔLRR were created by PCR amplification of full-length GS2-IpaH9.8 and truncated IpaH9.8ΔLRR, respectively, with primers that introduced NcoI and NotI (GS2-IpaH9.8) or NheI and NotI (IpaH9.8 ΔLRR) sites, after which the resulting PCR products were ligated into pET24d(+). Plasmid pET28a-GS2 was created by PCR amplification of GS2 from pHFT2-GS2 using primers that introduced an upstream NcoI site and downstream FLAG, 6x-His, and *Hin*dIII sequences, after which the resulting PCR product was ligated into pET28a(+). Plasmid pTriEx-3-GS2-IpaH9.8^{C337A} was created by PCR amplification of GS2-IpaH9.8^{C337A} from pcDNA3-GS2-IpaH9.8^{C337A} with primers that introduced EcoRV and *Hin*dIII sites, after which the resulting PCR product was ligated into pTriEx-3. Plasmid pET28a-EGFP was created by PCR amplification of GFP with primers adding C-terminal 6x-His tag, after which the resulting PCR product was ligated in pET28a(+). All plasmids were verified by DNA sequencing at the Cornell Biotechnology Resource Center (BRC).

Cell Lines, Culture, and Transfection. All cell lines used in this study are provided in Supplementary Table 2. Briefly, HEK293T and HeLa cells were obtained from ATCC, HeLa H2B-EGFP cells were kindly provided by Elena Nigg, and MCF10A rtTA cells were kindly provided by Matthew Paszek, HEK293T, HeLa, and HeLa H2B-EGFP cells were cultured in DMEM with 4.5 g/L glucose and L-glutamine (VWR) supplemented with 10% FetalCloneI (VWR) and 1% penicillin-streptomycin-amphotericin B (ThermoFisher) MCF-10a cells were grown in DMEM/F12 media (ThermoFisher) supplemented with 5% horse serum (ThermoFisher), 20 ng/mL EGF (Peprotech), 0.5 mg/mL hydrocortisone (Sigma), 100 ng/mL cholera toxin (Sigma), 10 μg/mL insulin (Sigma), and 1% penicillin-streptomycin-amphotericin B (ThermoFisher). All cells were maintained at 37 °C, 5% CO_2 and 90% relative humidity (RH).

Stable MCF10A rtTA cell lines were generated using Nucleofection kit V (Lonza) and HyPBase, an expression plasmid for the hyperactive version of the PiggyBac transposase. Transposition of MCF10A rtTA cells was performed to generate the following stable lines: MCF10A EGFP-HRas^{G12V}; MCF10A EGFP-HRas^{G12V}:GS2-IpaH9.8; MCF10A EGFP-HRas^{G12V}:GS2-IpaH9.8^{C337A}; and MCF10A GS2-IpaH9.8. Stable cell lines were selected using 200 μg/mL hygromycin B (ThermoFisher).

Stable HEK293T cell lines expressing EGFP, EGFP-HRas^{G12V}, ERK2-EGFP, d2EGFP were generated by lentiviral transformation. Specifically, pLV IRES eGFP, pcDH1 eGFP-HRas^{G12V}, pcDH1 ERK2-EGFP, or pHIV-d2EGFP were transfected into HEK293T cells along with psPAX2 and pMD2.G by calcium phosphate transfection. Media was replaced after ∼16 h, followed by a 48-h incubation to allow virus production. Viral supernatant was removed and Polybrene (Sigma-Aldrich) added to a final concentration of 8 μg/mL, followed by clearance of cell debris by centrifugation at 2000 rpm for 5 min. Resultant supernatant was diluted 1:6 with cell media and added to previously plated HEK293T cells for stable integration. HEK293T EGFP and HEK293T ERK2-EGFP cell lines were selected by fluorescence activated cell sorting (BD FACSAria). The HEK293T EGFP-HRas^{G12V} cell line was selected using 1 μg/mL puromycin (Sigma-Aldrich).

Western Blot Analysis. HEK293T cells were plated at 10 000 cells/cm^2 and transfected as described above before lysis with RIPA lysis buffer (Thermo Fisher). MCF10A cells were plated at 20 000 cells/cm^2 and induced with 0.2 μg/mL doxycycline for 24 h before lysis with cell lysis buffer. Lysates were separated on Any kD polyacrylamide gels (Bio-Rad) and transferred to PVDF membranes. α-HIS-HRP (Abcam), α-GFP (Krackeler), and α-GAPDH (Millipore) antibodies were diluted 1:5000 and in TBST + 1% milk and incubated for 1 h at room temperature. Secondary antibody goat antimouse IgG with HRP conjugation (Promega) was diluted at 1:2,500 and used as needed.

Flow Cytometric Analysis. Cells were passed into 12-well plates at 10 000 cells/cm^2. 16−24 h after seeding, cells were transiently transfected with 1 μg total DNA at a 1:2 ratio of DNA:jetPrime (Polyplus Transfection). Cells were transfected with 0.05 μg of target, 0.25 μg of ubiquibody or control, and balanced with empty pcDNA3 vector. Culture media was replaced 4−6 h post-transfection. Then, 24 h post-transfection, cells were harvested and resuspended in phosphate buffered saline (PBS) for analysis using a FACSCalibur or FACSAria Fusion (BD Biosciences). FlowJo Version 10 was used to analyze samples by geometric mean fluorescence determined from 10 000 events.

Microscopy. Cells were plated at 10 000 cells/cm^2 on a glass bottom 12-well plate pretreated with poly-L-lysine (Sigma-Aldrich). After seeding for 16−24 h, cells were transfected with 1 μg total DNA at a 1:2 ratio of DNA:jetPrime (Polyplus Transfection). cells were transfected with 0.05 μg of target, 0.25 μg of ubiquibody or control, and balanced with empty pcDNA3 vector. Culture media was replaced 4−6 h post-transfection. Then, 24 h post-transfection, cells were fixed with 4% paraformaldehyde. For EGFR-EGFP samples, cells were blocked with 5% normal goat serum in PBS for 2 h at room temperature. The anti-EGFR antibody (Cell Signaling #4267) was diluted 1:200 in 5% normal goat serum in PBS and incubated overnight at 4 °C. Cells were washed three times with PBS, then incubated for 1 h at room

DOI: 10.1021/acscentsci.9b00127
ACS Cent. Sci. 2019, 5, 852−866

temperature with antirabbit-AF647 diluted 1:200 in 5% normal goat serum in PBS. Cells were washed three times with PBS. Cell nuclei were stained with Hoescht diluted 1:10 000 in PBS for 10 min, then washed three times in PBS. Samples were imaged on a inverted Zeiss LSM88-confocal/multiphoton microscope (i880) using a 40× water immersion objective. Images were analyzed with FIJI.

Protein Expression and Purification. Purified proteins were obtained by growing *E. coli* BL21(DE3) cells containing a pET28a-based plasmid encoding the desired protein or Rosetta (DE3) cells containing a pTriEx-3-based plasmid in 200 mL of Luria−Bertani (LB) medium at 37 °C. Expression was induced with 0.1 mM IPTG when the culture density (Abs_{600}) reached 0.6−0.8 and growth continued for 6 h at 30 °C. Cultures were harvested by centrifugation at 4000*g* for 30 min at 4 °C. Cell pellets were stored at −20 °C overnight. Thawed pellets were resuspended in 10 mL equilibration buffer (25 mM Tris-HCl, pH 7.4, 500 mM NaCl and 20 mM imidazole) and lysed with a high-pressure homogenizer (Avestin Emulsi-Flex C5). The insoluble fraction was cleared by centrifugation at 12000*g* for 30 min at 4 °C. His-tagged protein was purified by gravity flow using 500 μL HisPur Ni-NTA resin (ThermoFisher). The soluble fraction was passed through the resin, after which the resin was washed with 3 mL of wash buffer (25 mM Tris-HCl, pH 7.4, 500 mM NaCl and 50 mM imidazole). Protein was eluted with 1.5 mL elution buffer (25 mM Tris-HCl, pH 7.4, 500 mM NaCl, and 250 mM imidazole). Purified fractions were desalted and concentrated (Pierce PES Protein Concentrators).

ELISA. A 96-well enzyme immunoassay plate was coated with 100 μL of EGFP at 10 μg/mL in 0.05 M $NaCO_3$ buffer, pH 9.6 at 4 °C overnight. The plate was then washed three times 200 μL PBST (1× PBS + 0.1% Tween 20) per well and blocked with 250 μL PBS with 3% milk per well at room temperature for 3 h, slowly mixing. The plate was washed three more times, followed by the addition of serial dilutions of purified proteins in blocking buffer at 60 μL per well. Plate was incubated at room temperature, slowly mixing for 1 h. The plate was washed three times to remove unbound protein and then incubated with 50 μL/well of anti-FLAG (DDDYK) antibody conjugated to horseradish peroxidase (HRP) diluted 1:10,000 in PBST + 1% milk for 1 h with slow mixing. The plate was washed three times before the addition of 50 μL/well 1-Step Ultra TMB (3,3′,5,5′-tetramethylbenzidine) (ThermoFisher). The reaction was allowed to incubate with slow mixing and then quenched with 50 μL/well of 3N H_2SO_4. The quenched plate was then read at 450 nm.

Synthesis and Characterization of Cationic Polypeptides. N4 (TEP) polyamines were synthesized as we described recently[37] according to a modified procedure of Uchida and co-workers.[59] Briefly, to a chilled solution of poly(β-benzyl-L-aspartate) in *N*-methyl-2-pyrrolidone (NMP) (Sigma) (2 mL) was added dropwise with stirring 50 equiv of tetraethylenepentamine (Sigma) diluted 2-fold with NMP. After stirring for 2 h at 0 °C, the pH was adjusted to 1 with dropwise addition while stirring of cold 6 N HCl. The resulting solution was dialyzed from a regenerated cellulose membrane bag (Spectrum Laboratories, 1 kDa MWCO) against 0.01 N HCl followed by distilled water, frozen, and lyophilized to give a white powder. Polyamines used in this study were characterized by ^{1}H NMR spectra in deuterium oxide (Cambridge Isotope Laboratories) using a Bruker Avance 400 MHz NMR spectrometer at 25 °C: ^{1}H NMR (400 MHz, D2O) δ 4.72 (s, 1H), 3.64−3.39 (m, 9H), 3.37−3.05 (m, 5H), 3.00−2.62 (m, 4H).

Preparation of mRNA by in Vitro Transcription. cDNA encoding uAbs was cloned into pGEM4Z/GFP/A64 by replacing the GFP fragment with XbaI and NotI sites. Additionally, the human α-globin 3′ UTR sequence was placed between the cDNA and the poly A tail using NotI and *Eco*RI to improve mRNA translation. Linearization with SpeI, followed by in vitro transcription (IVT) with HiScribe T7 High Yield RNA synthesis kit (NEB), yielded a transcript containing 64 nucleotides of vector-derived sequence, the coding sequence, α-globin 3′ UTR, and 64 A residues. In a typical 20 μL reaction, the following nucleotides were prepared: ATP (10 mM), pseudo-UTP (10 mM), methyl-CTP (10 mM), GTP (2 mM), antireverse Cap analogue (8 mM, NEB). RNA was purified by RNeasy purification kit (Qiagen, Hilden, Germany). RNA quality was confirmed by running a 1% agarose gel. Concentration was determined by Abs_{260}.

Nanoplex Transfection. Polyamines were dissolved in 10 mM HEPES buffer (pH 7.4). For each well of a 96-well plate, 200 ng of mRNA diluted in 5 μL of OptiMEM (Thermo Fisher) was mixed with 5 μL of OptiMEM containing PABP (mRNA/PABP weight ratio = 1:5) at room temperature for 10 min. Afterward, 5 μL OptiMEM containing polyamines was added and incubated at room temperature for 15 min prior to transfection into HEK293T stably expressing d2EGFP. Polyamines were adjusted to achieve 50 to 1 (N/P) ratio for transfection. EGFP expression was measured by BD FACSCelesta (Becton Dickinson) at different time points after transfection.

Animal Experiments. Mouse care and experimental procedures were performed under pathogen-free conditions in accordance with established institutional guidelines and approved protocols from the MIT Division of Comparative Medicine. C57BL/6-Tg(UBC-GFP)30Scha/J mice were purchased from Jackson Laboratory. 8−10 week-old mice were injected subcutaneously in ears with 5 μg of mRNA and 25 μg of PABP packaged with N4 (TEP) polyamines in a volume of 25 μL of OptiMEM under anesthesia. Fluorescent imaging was performed with a CCD camera mounted in a light-tight specimen box (Xenogen). The exposure time was 1 s. Imaging and quantification of signals were controlled by Living Image acquisition and analysis software (Xenogen).

Statistical Analysis. For in vitro and in vivo studies, *p* values were determined by paired sample *t*-test.

Safety Statement. No unexpected or unusually high safety hazards were encountered in the course of this work.

■ ASSOCIATED CONTENT

Supporting Information

The Supporting Information is available free of charge on the ACS Publications website at DOI: 10.1021/acscentsci.9b00127.

List of E3 ubiquitin ligases, list of strains and plasmids, flow cytometry histograms, characterization of GS2-IpaH9.8 binding activity and expression, additional data on degradation of GFP variants and FP fusions, data on activity of alternative GFP-binding domains, and data on activity of GS2-IpaH9.8 in stable cell lines (PDF)

DOI: 10.1021/acscentsci.9b00127
ACS Cent. Sci. 2019, 5, 852−866

AUTHOR INFORMATION

Corresponding Author

*Tel: 607-254-8560. E-mail: md255@cornell.edu.

ORCID

Jiahe Li: 0000-0002-9889-8546
Richard W. Roberts: 0000-0002-8587-5097
Shohei Koide: 0000-0001-5473-4358
Paula T. Hammond: 0000-0002-9835-192X
Matthew P. DeLisa: 0000-0003-3226-1566

Author Contributions

#M.B.L. and J.L. contributed equally to this work.

Author Contributions

M.B.L. designed all the research, performed all the research, analyzed data, and wrote the paper. J.L. designed, performed, and analyzed all research related to nanoplex delivery. E.A.S. performed research related to the design and evaluation of ubiquibodies. J.L. and P.T.H. conceptualized and developed key concepts on nanoplex delivery and experimental design for the mRNA/PABP protein complex and synthetic design of polypeptides for the polyplex system. W.E.E., R.W.R., and P.T.H. developed key constructs and reagents, and contributed to experimental design. M.P.D. conceptualized the project, designed research, analyzed data, and wrote the paper.

Notes

The authors declare no competing financial interest.

ACKNOWLEDGMENTS

We thank Anne Messer, Byung Kangwon, Cam Patterson, Elena Nigg, Gregory Martin, Karel Svoboda, Markus Affolter, Matthew Paszek, Melanie Cobb, Pengbo Zhou, Didier Trono, Valerie Weaver, Jon Lakins, Alan Bradley, Michael Davidson, Jan Lammerding, and Smita Nair for kindly providing plasmids encoding genes used in this study. We also thank Yuxin Mao for providing *L. pneumophila* gDNA, Yung Fu for providing EHEC and *S. typhimurium* gDNA, and Adam Bogdanave for providing *X. campestris* gDNA. This work was supported by the National Science Foundation Grant CBET-0449080 (to M.P.D.), the National Institutes of Health Grant Numbers CA132223 (to M.P.D.), CA170820 and GM083898 (to R.W.R.), CA194864 and CA212608 (to S.K.) the New York State Office of Science, Technology and Academic Research Distinguished Faculty Award (to M.P.D.), the Cornell Technology Acceleration and Maturation (CTAM) Fund, the National Science Foundation Graduate Research Fellowship Program Grants DGE-1650441 (to M.B.L.) and DGE-1144153 (to E.A.S.), Cornell Presidential Life Science Fellowships (to M.B.L. and E.A.S.), a Cornell Fleming Graduate Scholarship (to M.B.L.), the Koch Institute Support Grant P30-CA14051 from the National Cancer Institute and the Department of Defense Ovarian Cancer Research Program Teal Innovator Award (to P.T.H.). Confocal microscopy was supported by NYSTEM Grant CO29155 and NIH Grant S10OD018516 and FACS analysis was supported by the Cornell Biotechnology Resource Center and the David H. Koch Institute Flow Cytometry Core at MIT.

REFERENCES

(1) McManus, M. T.; Sharp, P. A. Gene silencing in mammals by small interfering RNAs. *Nat. Rev. Genet.* **2002**, *3* (10), 737−747.

(2) Deleavey, G. F.; Damha, M. J. Designing chemically modified oligonucleotides for targeted gene silencing. *Chem. Biol.* **2012**, *19* (8), 937−954.

(3) Boettcher, M.; McManus, M. T. Choosing the right tool for the job: RNAi, TALEN, or CRISPR. *Mol. Cell* **2015**, *58* (4), 575−585.

(4) Gaj, T.; Gersbach, C. A.; Barbas, C. F., 3rd ZFN, TALEN, and CRISPR/Cas-based methods for genome engineering. *Trends Biotechnol.* **2013**, *31* (7), 397−405.

(5) Cox, D. B.; Platt, R. J.; Zhang, F. Therapeutic genome editing: prospects and challenges. *Nat. Med.* **2015**, *21* (2), 121−131.

(6) Soutschek, J.; Akinc, A.; Bramlage, B.; Charisse, K.; Constien, R.; Donoghue, M.; Elbashir, S.; Geick, A.; Hadwiger, P.; Harborth, J.; John, M.; Kesavan, V.; Lavine, G.; Pandey, R. K.; Racie, T.; Rajeev, K. G.; Rohl, I.; Toudjarska, I.; Wang, G.; Wuschko, S.; Bumcrot, D.; Koteliansky, V.; Limmer, S.; Manoharan, M.; Vornlocher, H. P. Therapeutic silencing of an endogenous gene by systemic administration of modified siRNAs. *Nature* **2004**, *432* (7014), 173−178.

(7) Bumcrot, D.; Manoharan, M.; Koteliansky, V.; Sah, D. W. RNAi therapeutics: a potential new class of pharmaceutical drugs. *Nat. Chem. Biol.* **2006**, *2* (12), 711−719.

(8) Wang, M.; Glass, Z. A.; Xu, Q. Non-viral delivery of genome-editing nucleases for gene therapy. *Gene Ther.* **2017**, *24* (3), 144−150.

(9) Buetow, L.; Huang, D. T. Structural insights into the catalysis and regulation of E3 ubiquitin ligases. *Nat. Rev. Mol. Cell Biol.* **2016**, *17* (10), 626−642.

(10) Neklesa, T. K.; Winkler, J. D.; Crews, C. M. Targeted protein degradation by PROTACs. *Pharmacol. Ther.* **2017**, *174*, 138−144.

(11) Deshaies, R. J. Protein degradation: Prime time for PROTACs. *Nat. Chem. Biol.* **2015**, *11* (9), 634−635.

(12) Schneekloth, J. S., Jr.; Fonseca, F. N.; Koldobskiy, M.; Mandal, A.; Deshaies, R.; Sakamoto, K.; Crews, C. M. Chemical genetic control of protein levels: selective in vivo targeted degradation. *J. Am. Chem. Soc.* **2004**, *126* (12), 3748−3754.

(13) Hines, J.; Gough, J. D.; Corson, T. W.; Crews, C. M. Posttranslational protein knockdown coupled to receptor tyrosine kinase activation with phosphoPROTACs. *Proc. Natl. Acad. Sci. U. S. A.* **2013**, *110* (22), 8942−8947.

(14) Schneekloth, A. R.; Pucheault, M.; Tae, H. S.; Crews, C. M. Targeted intracellular protein degradation induced by a small molecule: En route to chemical proteomics. *Bioorg. Med. Chem. Lett.* **2008**, *18* (22), 5904−5908.

(15) Bondeson, D. P.; Mares, A.; Smith, I. E.; Ko, E.; Campos, S.; Miah, A. H.; Mulholland, K. E.; Routly, N.; Buckley, D. L.; Gustafson, J. L.; Zinn, N.; Grandi, P.; Shimamura, S.; Bergamini, G.; Faelth-Savitski, M.; Bantscheff, M.; Cox, C.; Gordon, D. A.; Willard, R. R.; Flanagan, J. J.; Casillas, L. N.; Votta, B. J.; Den Besten, W.; Famm, K.; Kruidenier, L.; Carter, P. S.; Harling, J. D.; Churcher, I.; Crews, C. M. Catalytic in vivo protein knockdown by small-molecule PROTACs. *Nat. Chem. Biol.* **2015**, *11* (8), 611−617.

(16) Sakamoto, K. M.; Kim, K. B.; Kumagai, A.; Mercurio, F.; Crews, C. M.; Deshaies, R. J. Protacs: chimeric molecules that target proteins to the Skp1-Cullin-F box complex for ubiquitination and degradation. *Proc. Natl. Acad. Sci. U. S. A.* **2001**, *98* (15), 8554−8559.

(17) Buckley, D. L.; Crews, C. M. Small-molecule control of intracellular protein levels through modulation of the ubiquitin proteasome system. *Angew. Chem., Int. Ed.* **2014**, *53* (9), 2312−2330.

(18) Osherovich, L. Degradation from within. *Science-Business Exchange* **2014**, *7*, 191.

(19) Zhou, P.; Bogacki, R.; McReynolds, L.; Howley, P. M. Harnessing the ubiquitination machinery to target the degradation of specific cellular proteins. *Mol. Cell* **2000**, *6* (3), 751−756.

(20) Zhang, J.; Zheng, N.; Zhou, P. Exploring the functional complexity of cellular proteins by protein knockout. *Proc. Natl. Acad. Sci. U. S. A.* **2003**, *100* (24), 14127−14132.

(21) Hatakeyama, S.; Watanabe, M.; Fujii, Y.; Nakayama, K. I. Targeted destruction of c-Myc by an engineered ubiquitin ligase suppresses cell transformation and tumor formation. *Cancer Res.* **2005**, *65* (17), 7874−7879.

DOI: 10.1021/acscentsci.9b00127
ACS Cent. Sci. 2019, 5, 852−866

(22) Ma, Y.; Gu, Y.; Zhang, Q.; Han, Y.; Yu, S.; Lu, Z.; Chen, J. Targeted degradation of KRAS by an engineered ubiquitin ligase suppresses pancreatic cancer cell growth in vitro and in vivo. *Mol. Cancer Ther.* **2013**, *12* (3), 286−294.
(23) Kong, F.; Zhang, J.; Li, Y.; Hao, X.; Ren, X.; Li, H.; Zhou, P. Engineering a single ubiquitin ligase for the selective degradation of all activated ErbB receptor tyrosine kinases. *Oncogene* **2014**, *33* (8), 986−995.
(24) Sufan, R. I.; Moriyama, E. H.; Mariampillai, A.; Roche, O.; Evans, A. J.; Alajez, N. M.; Vitkin, I. A.; Yang, V. X.; Liu, F. F.; Wilson, B. C.; Ohh, M. Oxygen-independent degradation of HIF-alpha via bioengineered VHL tumour suppressor complex. *EMBO Mol. Med.* **2009**, *1* (1), 66−78.
(25) Portnoff, A. D.; Stephens, E. A.; Varner, J. D.; DeLisa, M. P. Ubiquibodies, synthetic E3 ubiquitin ligases endowed with unnatural substrate specificity for targeted protein silencing. *J. Biol. Chem.* **2014**, *289* (11), 7844−7855.
(26) Caussinus, E.; Kanca, O.; Affolter, M. Fluorescent fusion protein knockout mediated by anti-GFP nanobody. *Nat. Struct. Mol. Biol.* **2012**, *19* (1), 117−121.
(27) Fulcher, L. J.; Hutchinson, L. D.; Macartney, T. J.; Turnbull, C.; Sapkota, G. P. Targeting endogenous proteins for degradation through the affinity-directed protein missile system. *Open Biol.* **2017**, *7* (5), 170066.
(28) Fulcher, L. J.; Macartney, T.; Bozatzi, P.; Hornberger, A.; Rojas-Fernandez, A.; Sapkota, G. P. An affinity-directed protein missile system for targeted proteolysis. *Open Biol.* **2016**, *6* (10), 160255.
(29) Shin, Y. J.; Park, S. K.; Jung, Y. J.; Kim, Y. N.; Kim, K. S.; Park, O. K.; Kwon, S. H.; Jeon, S. H.; Trinh le, A.; Fraser, S. E.; Kee, Y.; Hwang, B. J. Nanobody-targeted E3-ubiquitin ligase complex degrades nuclear proteins. *Sci. Rep.* **2015**, *5*, 14269.
(30) Kanner, S. A.; Morgenstern, T.; Colecraft, H. M. Sculpting ion channel functional expression with engineered ubiquitin ligases. *eLife* **2017**, *6*, No. e29744.
(31) Baltz, M. R.; Stephens, E. A.; DeLisa, M. P. Design and functional characterization of synthetic E3 ubiquitin ligases for targeted protein depletion. *Curr. Protoc Chem. Biol.* **2018**, *10* (1), 72−90.
(32) Maculins, T.; Fiskin, E.; Bhogaraju, S.; Dikic, I. Bacteria-host relationship: ubiquitin ligases as weapons of invasion. *Cell Res.* **2016**, *26* (4), 499−510.
(33) Lin, Y. H.; Machner, M. P. Exploitation of the host cell ubiquitin machinery by microbial effector proteins. *J. Cell Sci.* **2017**, *130* (12), 1985−1996.
(34) Zhu, Y.; Li, H.; Hu, L.; Wang, J.; Zhou, Y.; Pang, Z.; Liu, L.; Shao, F. Structure of a Shigella effector reveals a new class of ubiquitin ligases. *Nat. Struct. Mol. Biol.* **2008**, *15* (12), 1302−1308.
(35) Singer, A. U.; Schulze, S.; Skarina, T.; Xu, X.; Cui, H.; Eschen-Lippold, L.; Egler, M.; Srikumar, T.; Raught, B.; Lee, J.; Scheel, D.; Savchenko, A.; Bonas, U. A pathogen type III effector with a novel E3 ubiquitin ligase architecture. *PLoS Pathog.* **2013**, *9* (1), No. e1003121.
(36) Rohde, J. R.; Breitkreutz, A.; Chenal, A.; Sansonetti, P. J.; Parsot, C. Type III secretion effectors of the IpaH family are E3 ubiquitin ligases. *Cell Host Microbe* **2007**, *1* (1), 77−83.
(37) Li, J.; He, Y.; Wang, W.; Wu, C.; Hong, C.; Hammond, P. T. Polyamine-mediated stoichiometric assembly of ribonucleoproteins for enhanced mRNA delivery. *Angew. Chem., Int. Ed.* **2017**, *56* (44), 13709−13712.
(38) Ashida, H.; Kim, M.; Schmidt-Supprian, M.; Ma, A.; Ogawa, M.; Sasakawa, C. A bacterial E3 ubiquitin ligase IpaH9.8 targets NEMO/IKKgamma to dampen the host NF-kappaB-mediated inflammatory response. *Nat. Cell Biol.* **2010**, *12* (1), 66−73.
(39) Li, P.; Jiang, W.; Yu, Q.; Liu, W.; Zhou, P.; Li, J.; Xu, J.; Xu, B.; Wang, F.; Shao, F. Ubiquitination and degradation of GBPs by a Shigella effector to suppress host defence. *Nature* **2017**, *551* (7680), 378−383.
(40) Koide, A.; Wojcik, J.; Gilbreth, R. N.; Hoey, R. J.; Koide, S. Teaching an old scaffold new tricks: monobodies constructed using alternative surfaces of the FN3 scaffold. *J. Mol. Biol.* **2012**, *415* (2), 393−405.
(41) Koide, A.; Gilbreth, R. N.; Esaki, K.; Tereshko, V.; Koide, S. High-affinity single-domain binding proteins with a binary-code interface. *Proc. Natl. Acad. Sci. U. S. A.* **2007**, *104* (16), 6632−6637.
(42) Tsien, R. Y. The green fluorescent protein. *Annu. Rev. Biochem.* **1998**, *67*, 509−544.
(43) Shaner, N. C.; Steinbach, P. A.; Tsien, R. Y. A guide to choosing fluorescent proteins. *Nat. Methods* **2005**, *2* (12), 905−909.
(44) Khmelinskii, A.; Meurer, M.; Ho, C. T.; Besenbeck, B.; Fuller, J.; Lemberg, M. K.; Bukau, B.; Mogk, A.; Knop, M. Incomplete proteasomal degradation of green fluorescent proteins in the context of tandem fluorescent protein timers. *Mol. Biol. Cell* **2016**, *27* (2), 360−370.
(45) Saerens, D.; Pellis, M.; Loris, R.; Pardon, E.; Dumoulin, M.; Matagne, A.; Wyns, L.; Muyldermans, S.; Conrath, K. Identification of a universal VHH framework to graft non-canonical antigen-binding loops of camel single-domain antibodies. *J. Mol. Biol.* **2005**, *352* (3), 597−607.
(46) Sha, F.; Gencer, E. B.; Georgeon, S.; Koide, A.; Yasui, N.; Koide, S.; Hantschel, O. Dissection of the BCR-ABL signaling network using highly specific monobody inhibitors to the SHP2 SH2 domains. *Proc. Natl. Acad. Sci. U. S. A.* **2013**, *110* (37), 14924−14929.
(47) Cetin, M.; Evenson, W. E.; Gross, G. G.; Jalali-Yazdi, F.; Krieger, D.; Arnold, D.; Takahashi, T. T.; Roberts, R. W. RasIns: genetically encoded intrabodies of activated Ras proteins. *J. Mol. Biol.* **2017**, *429* (4), 562−573.
(48) Schaefer, B. C.; Schaefer, M. L.; Kappler, J. W.; Marrack, P.; Kedl, R. M. Observation of antigen-dependent CD8+ T-cell/dendritic cell interactions in vivo. *Cell. Immunol.* **2001**, *214* (2), 110−122.
(49) Norkowski, S.; Schmidt, M. A.; Ruter, C. The species-spanning family of LPX-motif harbouring effector proteins. *Cell. Microbiol.* **2018**, *20* (11), No. e12945.
(50) Ashida, H.; Sasakawa, C. Shigella IpaH family effectors as a versatile model for studying pathogenic bacteria. *Front. Cell. Infect. Microbiol.* **2016**, *5*, 100.
(51) Metzger, M. B.; Hristova, V. A.; Weissman, A. M. HECT and RING finger families of E3 ubiquitin ligases at a glance. *J. Cell Sci.* **2012**, *125*, 531−537.
(52) Crews, C. M. Targeting the undruggable proteome: the small molecules of my dreams. *Chem. Biol.* **2010**, *17* (6), 551−555.
(53) Arkin, M. R.; Wells, J. A. Small-molecule inhibitors of protein-protein interactions: progressing towards the dream. *Nat. Rev. Drug Discovery* **2004**, *3* (4), 301−317.
(54) Adams, D.; Gonzalez-Duarte, A.; O'Riordan, W. D.; Yang, C. C.; Ueda, M.; Kristen, A. V.; Tournev, I.; Schmidt, H. H.; Coelho, T.; Berk, J. L.; Lin, K. P.; Vita, G.; Attarian, S.; Plante-Bordeneuve, V.; Mezei, M. M.; Campistol, J. M.; Buades, J.; Brannagan, T. H., 3rd; Kim, B. J.; Oh, J.; Parman, Y.; Sekijima, Y.; Hawkins, P. N.; Solomon, S. D.; Polydefkis, M.; Dyck, P. J.; Gandhi, P. J.; Goyal, S.; Chen, J.; Strahs, A. L.; Nochur, S. V.; Sweetser, M. T.; Garg, P. P.; Vaishnaw, A. K.; Gollob, J. A.; Suhr, O. B. Patisiran, an RNAi therapeutic, for hereditary transthyretin amyloidosis. *N. Engl. J. Med.* **2018**, *379* (1), 11−21.
(55) Fu, Y.; Foden, J. A.; Khayter, C.; Maeder, M. L.; Reyon, D.; Joung, J. K.; Sander, J. D. High-frequency off-target mutagenesis induced by CRISPR-Cas nucleases in human cells. *Nat. Biotechnol.* **2013**, *31* (9), 822−826.
(56) Fedorov, Y.; Anderson, E. M.; Birmingham, A.; Reynolds, A.; Karpilow, J.; Robinson, K.; Leake, D.; Marshall, W. S.; Khvorova, A. Off-target effects by siRNA can induce toxic phenotype. *RNA* **2006**, *12* (7), 1188−1196.
(57) Colwill, K.; Renewable Protein Binder Working Group; Graslund, S. A roadmap to generate renewable protein binders to the human proteome. *Nat. Methods* **2011**, *8* (7), 551−558.
(58) Guan, S.; Rosenecker, J. Nanotechnologies in delivery of mRNA therapeutics using nonviral vector-based delivery systems. *Gene Ther.* **2017**, *24* (3), 133−143.

DOI: 10.1021/acscentsci.9b00127
ACS Cent. Sci. 2019, 5, 852−866

(59) Uchida, H.; Itaka, K.; Nomoto, T.; Ishii, T.; Suma, T.; Ikegami, M.; Miyata, K.; Oba, M.; Nishiyama, N.; Kataoka, K. Modulated protonation of side chain aminoethylene repeats in N-substituted polyaspartamides promotes mRNA transfection. *J. Am. Chem. Soc.* **2014**, *136* (35), 12396−12405.

DOI: 10.1021/acscentsci.9b00127
ACS Cent. Sci. 2019, 5, 852−866